Chapter 15

A Unified Approach to the Problems of Semiconductor Laser Theory

M. J. Adams

15.1 INTRODUCTION

This chapter is concerned with some of the fundamental problems of semiconductor laser theory; more specifically, let us ask the questions:

(i) *which problems remain to be solved?*
(ii) *of the remainder, which solutions are the most appropriate for given situations?*
(iii) *how much influence on laser development have the theoretical solutions had?*

A conventional starting-point would be to discuss the historical progress of the laser from the early days of a low-power, high-threshold device requiring pulsed operation and/or a low-temperature environment, to the current situation of a wide variety of laser structures adapted for CW room-temperature operation, good mode control, ease of modulation, etc. A brief history of theoretical topics should include (chronologically) the reasons for high thresholds, the temperature dependence of threshold current, the role of dielectric waveguiding, the problem of heat dissipation, the gain-current relationship, transient behaviour (noise, resonance frequencies, 'spiking', modulation, time delays, Q-switching), electromagnetic mode control, carrier transport phenomena and many other topics.

However, rather than following along the lines suggested in the preceding paragraph, I propose to take a more formal approach and discuss these topics in an ordered way, as shown in Table 15.1. The table contains three columns headed respectively 'electrons', 'photons', and 'phonons', and five rows labelled 'x-direction', 'y-direction', 'z-direction', 'time', and 'energy'. The object of this structure is to categorize each fundamental effect associated with a particular set of quasi-particles by its spatial, temporal and spectral behaviour. Thus each available space in the Table contains an entry relating

Table 15.1 Fundamental physical phenomena in semiconductor lasers

	Electrons	Photons	Phonons
x-direction (normal to the junction plane)	carrier transport normal to the junctions	waveguiding normal to the junction plane	heat transfer from active layer to heat sink
y-direction (in the junction plane, parallel to the facets)	current spreading in the junction plane (associated with stripe 'architecture')	waveguiding associated with stripe 'architecture' (real or virtual guidance)	heat diffusion associated with stripe 'architecture'
z-direction (in the junction plane, perpendicular to the facets)	longitudinal carrier diffusion	longitudinal field distribution and its influence on catastrophic degradation	longitudinal temperature variations, stimulated Brillouin emission
time	modulation, 'spiking', noise effects in carrier currents, resonance, time delays, *Q*-switching	modulation, 'spiking', noise effects in lasing output, resonance, time delays, *Q*-switching	transient heating effects, long time delays
energy	band structure effects, impurity bands	spectral distribution of emission, selection rules, allowed transitions	non-radiative recombination associated with decreased efficiency, possible effects of long-term degradation

to one or more specific physical phenomena. In the next section some of these phenomena will be discussed in more detail, whilst in Section 15.3 some of the possible interactions between these effects will be explored. Finally in Section 15.4 the conclusions are summarized in the light of the three questions posed above.

15.2 THE FUNDAMENTAL PHYSICAL PHENOMENA

In this section the principal effects indicated in Table 15.1 will be dealt with in the order suggested by each column. The basic laser structure and spatial coordinates are indicated in Figure 15.1.

Figure 15.1 Schematic semiconductor laser structure and coordinate system

15.2.1 Electron effects

15.2.1.1 Spatial: x-direction

The simplest assumption, especially in the case of a double heterostructure laser with narrow active region, is that the carrier distributions are homogeneously distributed across the active layer. If this layer width is $2a$, then the rate of flow of carriers is simply given by $j/(2ea)$, where j is the current density and e is the electron charge. However, if a more detailed knowledge of the carrier distributions is needed, then the charge transport equations must be solved. Analytic solutions may be found only for situations of limited applicability where approximations are made to the full set of transport equations. Leaving aside the current controversy over the energy-band lineup at an abrupt heterojunction (1) and the somewhat vexed question of just

how 'abrupt' such an interface may be (2), the conventional approximations to the transport equations may be listed as:

(a) electron diffusion only (3–6),
(b) electron drift only (5),
(c) electron diffusion and drift (5),
(d) drift of electrons and holes (5).

In all cases these approximations ignore Poisson's equation and assume either constant or linear variation of electric field across the active region. Whilst approximation (a) may apply to widely-spaced heterojunctions, cases (a)–(c) are suitable for heavily-doped p-type active regions, and (d) applies to double injection in a lightly-doped active layer.

Numerical solutions of the charge transport equations describing the distribution of carriers in the x-direction (below threshold) have also been published for both homojunction (7) and double heterostructure (8) lasers. The results for the latter case would tend to indicate a uniform distribution of carriers across the greater part of the active layer, with fairly steep gradients close to each heterojunction. The possibility of carrier leakage into the adjacent passive layers has also been considered (9, 10). Carrier degeneracy effects may be included via the use of a generalized Einstein relation (11).

15.2.1.2 Spatial: y-direction

In Figure 15.1 the term stripe 'architecture' is used to indicate the structure in the y-direction which gives current control and electromagnetic mode confinement. The range of possible stripe configurations is now quite large, e.g. oxide-insulated, proton-bombarded, shallow and deep diffused, buried heterostructure, TJS, mesa, rib-guide, channelled-substrate, embedded stripe, etc. rather than specify a particular structure, we are concerned here to merely enumerate the carrier transport mechanisms of relevance and indicate the cases where theoretical solutions may be found. Perhaps the simplest and most general mechanism is that of lateral diffusion of electrons under a stripe contact; in this case the carrier distribution $n(y)$ is given by (12, 13):

$$n(y) = \begin{cases} \dfrac{jL_n^2}{2eaD_n}\left[1-\exp\left(-\dfrac{S}{L_n}\right)\cosh\left(\dfrac{y}{L_n}\right)\right] & \text{for } |y| \leqslant S \quad (15.1a) \\ \dfrac{jL_n^2}{2eaD_n}\sinh\left(\dfrac{S}{L_n}\right)\exp\left(-\dfrac{y}{L_n}\right) & \text{for } |y| > S \quad (15.1b) \end{cases}$$

where D_n is the diffusion constant, L_n the diffusion length, and $2S$ is the stripe width. More complicated situations will arise for specific stripe

configurations, especially those involving doping control. The effects of current spreading (14–19) and stimulated emission above threshold (13, 15, 17–20) have also been analysed. The results would indicate that the effects of stimulated emission are only important for wide stripes ($2S \gtrsim 15$ μm) (15, 19) whilst for narrow stripes ($2S \simeq 10$ μm) the distribution of carriers in the y-direction is largely determined by carrier diffusion and current spreading. A refined theory of current flow has recently been published (21), together with 'pioneering measurements' of the spatial variation of junction voltage.

15.2.1.3 Spatial: z-direction

Along the cavity length of the laser structure the conventional assumption is that of a uniform distribution of carriers below threshold. At threshold and above the distribution of carriers is closely coupled to that of the photon field, although longitudinal diffusion may be expected to oppose this effect and attempt to restore a uniform carrier distribution (22).

15.2.1.4 Temporal

Below threshold the temporal evolution of the carrier populations is governed by (at most) two simple rate equations; the intrinsic time delay before lasing commences is well known (23). Above threshold the interaction of photons and carriers leads to a dynamic situation and a wide range of interesting effects, the discussion of which will be postponed until Section 15.2.2.4.

15.2.1.5 Spectral

The electron energy states associated with lasing action may be those of the parabolic bands, of isolated impurity levels (24), or more usually of impurity bands which may or may not merge with the bands (25, 26). In high-purity material a number of states associated with excitons and many-body effects at high excitation level may also be involved (27). A detailed knowledge of the densities-of-states functions of the electrons and holes involved in lasing is essential for the calculation of recombination rates, gain-current relationships, emission spectra, etc. Further discussion of these effects is given at the appropriate point in Section 15.2.2.

15.2.2 Photon effects

15.2.2.1 Spatial: x-direction

The epitaxial layers indicated on the schematic laser structure of Figure 15.1 usually provide a dielectric waveguide due to the variation of refractive index in the x-direction (28). In order to describe this waveguide in the most general

Table 15.2 Homogeneous core waveguide results for the modes (real guidance)

Waveguide	Eigenvalue equation	Confinement factor
Asymmetric 3-layer slab	$2v(1-b)^{1/2} = N\pi + \tan^{-1}\left[\frac{b^{1/2}}{(1-b)^{1/2}}\right] + \tan^{-1}\left[\frac{(b+c)^{1/2}}{(1-b)^{1/2}}\right]$	$\Gamma = \frac{2v+b^{1/2}+\frac{(b+c')^{1/2}}{(1+c')}}{2v+\frac{1}{b^{1/2}}+\frac{1}{(b+c')^{1/2}}}$
Symmetric 5-layer slab	(i) $r \leqslant (1-b) \leqslant 1$ $v(1-b)^{1/2} \equiv \frac{N\pi}{2} + \tan^{-1}\left\{\left(\frac{1-b-r}{1-b}\right)^{1/2} \times \tan\left[\tan^{-1}\left(\frac{b^{1/2}}{(1-b-r)^{1/2}}\right) - v(1-b-r)^{1/2}\left(\frac{d}{a}-1\right)\right]\right\}$ (ii) $0 \leqslant (1-b) \leqslant r$ $v(1-b)^{1/2} \equiv \frac{N\pi}{2} + \tan^{-1}\left\{\left(\frac{r-1+b}{1-b}\right)^{1/2} \times \tanh\left[\tanh^{-1}\left(\frac{b^{1/2}}{(r-1+b)^{1/2}}\right) + v(r-1+b)^{1/2}\left(\frac{d}{a}-1\right)\right]\right\}$	$\Gamma = [v(1-b)^{1/2} + \sin v(1-b)^{1/2}\cos v(1-b)^{1/2}]$ $\times \left\{v(1-b)^{1/2} - \left(\frac{r}{1-b-r}\right)\sin v(1-b)^{1/2}\cos v(1-b)^{1/2} + v(1-b)^{1/2}\left(\frac{d}{a}-1+\frac{1}{vb^{1/2}}\right)\right\}^{-1}$ $\times \left[\cos^2 v(1-b)^{1/2} + \left(\frac{1-b}{1-b-r}\right)\sin^2 v(1-b)^{1/2}\right]^{-1}$

Notes:

(i) b is a normalized propagation constant: $b = \frac{(\beta/k)^2 - n_2^2}{n_1^2 - n_2^2}$, where β = longitudinal propagation constant, $k = 2\pi/\lambda$.

(ii) N is the mode number (0, 1, 2, ...).

(iii) For the three-layer slab, c' is defined in Equation 15.3; for the five-layer slab, r is defined in (15.6), and d/a in Figure 15.3.

(iv) The result for Γ for the five-layer slab was derived only for even-order modes.

terms it is convenient to express its properties in terms of normalized variables (28, 29), the most important of which is the normalized frequency, v (29), defined as:

$$v^2 = \left(\frac{a2\pi}{\lambda}\right)^2 (n_1^2 - n_2^2) \tag{15.2}$$

where a is the half-width of the guide (i.e. active layer), λ is the wavelength, n_1 is the refractive index of the active layer, and n_2 is the index of one adjacent layer (see inset of Figure 15.2). If n_3 is the refractive index of the passive layer on the other side of the active region, then an asymmetry factor c' may also be defined (28, 29):

$$c' = \frac{n_2^2 - n_3^2}{n_1^2 - n_2^2} \tag{15.3}$$

The parameters v and c' defined in Equations 15.2 and 15.3 completely specify a given dielectric slab waveguide with homogeneous 'core'. Numerical solutions of the wave equation and associated boundary conditions can then yield results for the propagation constants of the various modes. For the waveguide formed in a heterostructure laser, perhaps the most useful parameter which can be found from such a calculation is the radiation confinement factor, Γ (30), defined as the ratio of power confined in the core to the total power. Table 15.2 gives results for the eigenvalue equation and confinement factor for TE modes in the homogeneous core waveguide (29, 31). Figure 15.2 shows plots of Γ versus v for various values of the asymmetry factor c' (mode TE_0); Γ varies from zero at cut-off to unity at large values of v (corresponding to complete field confinement). The net gain per unit length (G) of a guided mode may be expressed in terms of the gain g in the active core layer and the loss α associated with the passive claddings as:

$$G = g\Gamma - \alpha(1-\Gamma) \tag{15.4}$$

This equation may be used to compute the threshold for lasing when G is just equal to the end-loss from the cavity facets.

A refinement of the simple three-layer slab waveguide structure has been the development of multilayer lasers (LGR (32, 33), SCH (34), SCHDFB (35, 36), leaky wave (37)) with separate optical and carrier confinement. A symmetric five-layer structure is shown schematically in the inset of Figure 15.3; the dielectric variation $\varepsilon(x)$ is given by:

$$\varepsilon(x) = \begin{cases} n_1^2 & \text{for } |x| \leqslant a \\ n_0^2 & \text{for } a < |x| \leqslant d \\ n_2^2 & \text{for } d < |x| \end{cases} \tag{15.5}$$

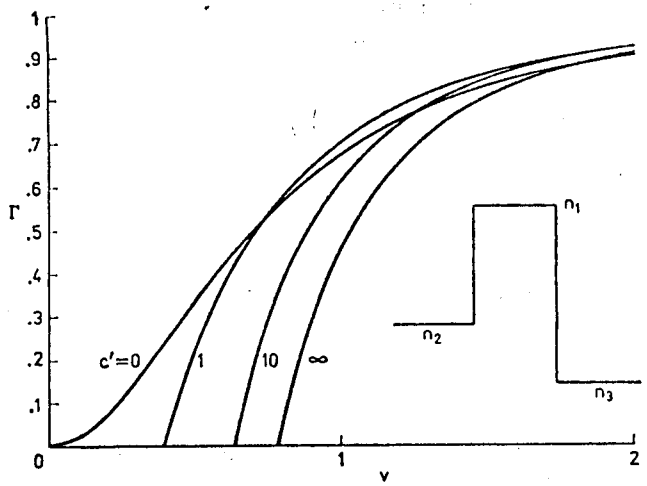

Figure 15.2 Radiation confinement factor Γ versus normalized frequency v for the lowest-order TE_0 mode of the asymmetric slab waveguide with homogeneous core; labelling parameter gives the value of the asymmetry factor c' defined in Equation 15.3

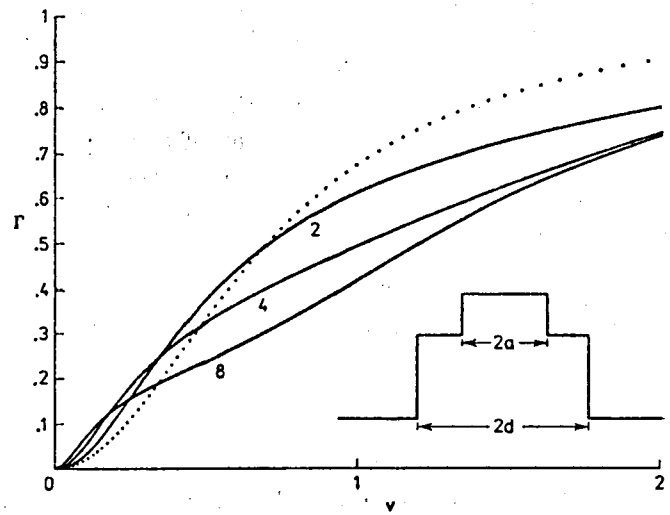

Figure 15.3 Γ versus v for the TE_0 mode of the five-layer symmetric slab waveguide (see inset) with $r = 1/3$ (defined as in Equation 15.6). Labelling parameter gives the value of the ratio d/a (see Equation 15.5). Broken line shows the variation of Γ with v for the equivalent three-layer slab ($d/a = 1$)

To analyse this structure it is convenient to retain the definition of v as in Equation 15.2, but to introduce a new measure of the asymmetry, defined as:

$$r = \frac{n_1^2 - n_0^2}{n_1^2 - n_2^2} \tag{15.6}$$

The parameters v, r and the ratio d/a are sufficient to completely specify a symmetric five-layer waveguide structure. Results for the eigenvalue equation for TE modes and the confinement factor (for even-order modes only) are given in Table 15.2. Plots of Γ versus v for $r = 1/3$ and $d/a = 2$, 4, and 8 are given in Figure 15.3 (solid lines). The broken line gives the variation of Γ for the equivalent three-layer slab ($d/a = 1$). For small v the values of Γ obtained with the five-layer structure are larger than those for the equivalent three-layer slab. Since at threshold the value of gain, g, is inversely dependent on Γ (cf. Equation 15.4), the result is a lower threshold for the SCH laser as compared with the equivalent DH device. Although the effect, as shown in Figure 15.3, is small, it is sufficient to produce worthwhile improvements; it may be augmented in practice by a superlinear gain-current relationship (32).

15.2.2.2 Spatial: y-direction

It was already noted in Section 15.2.1.2. that the stripe 'architecture' of Figure 15.1 would provide some degree of electromagnetic field confinement in the y-direction. In general there will be a complex dielectric waveguide, including variations of gain and loss as well as the refractive index, with a dielectric profile whose distribution in the y-direction depends on the details of the laser structure, drive current, etc. From a theoretical point of view therefore it is appropriate here to review the forms of dielectric profile for which solutions are known without the necessity of recourse to approximations or numerical techniques. For the case of real dielectric guides the symmetric profiles whose solutions are easily accessible are listed in Table 15.3; they are the step-index, linear, extended and cladded parabolic, exponential, and sech-squared waveguides. The assumption of symmetry in the y-direction seems well-founded, although it may sometimes be necessary also to consider some forms of asymmetry (38). Of the profiles listed in Table 15.3, only the step-index (39, 40), extended-parabolic (41, 42), and sech-squared (43–45) are applicable for the complex waveguide without the necessity of extensive computation.

As for the case of guidance in the x-direction (see 15.2.2.1 above) the waveguide parameter of greatest relevance to laser calculations is the confinement factor Γ. Since most of the newer laser structures are concerned

Table 15.3 Symmetric dielectric profiles with known solutions

Waveguide	Definition	Eigenvalue equation	Reference	v_{c1}
Step-index	$n^2(y) = \begin{cases} n_1^2, & \lvert y\rvert \leqslant a \\ n_2^2, & \lvert y\rvert > a \end{cases}$	$v(1-b)^{1/2} = \frac{N\pi}{2} + \tan^{-1}\left[\frac{b^{1/2}}{(1-b)^{1/2}}\right]$	28, 29, 31, 52, 53	1.57
Linear	$n^2(y) = \begin{cases} n_1^2\left[1-2\Delta\left\lvert\frac{y}{a}\right\rvert\right], & \lvert y\rvert \leqslant a \\ n_2^2 \equiv n_1^2[1-2\Delta], & \lvert y\rvert > a \end{cases}$	$\frac{Bi'((b-1)v^{2/3})}{Ai'((b-1)v^{2/3})} = \frac{Bi((b-1)v^{2/3})}{Ai((b-1)v^{2/3})}$ (odd); $\frac{Bi'((b-1)v^{2/3})}{Ai'((b-1)v^{2/3})} = \frac{Bi((b-1)v^{2/3})}{Ai((b-1)v^{2/3})}$ (even)	46–48	2.80
Extended-parabolic	$n^2(y) = n_1^2\left[1-2\Delta\left(\frac{y}{a}\right)^2\right]$ (all y)	$b = 1 - \frac{(2N+1)}{v}$	13, 38, 41, 42, 53	—
Cladded-parabolic	$n^2(y) = \begin{cases} n_1^2\left[1-2\Delta\left(\frac{y}{a}\right)^2\right], & \lvert y\rvert \leqslant a \\ n_2^2 \equiv n_1^2[1-2\Delta], & \lvert y\rvert > a \end{cases}$	Series solution	49	2.26
Exponential	$n^2(y) = n_1^2[1-2\Delta(1-e^{-\lvert y\rvert/a})]$	$J_{2vb^{1/2}}(2v) = 0$ (odd); $J'_{2vb^{1/2}}(2v) = 0$ (even)	3, 50–53	1.20
Sech-squared	$n^2(y) = n_2^2 + 2\Delta n_1^2 \operatorname{sech}^2\left(\frac{y}{a}\right)$	$b = \left[\frac{(1+4v^2)^{1/2} - (2N+1)}{2v}\right]^2$	43–45, 52–56	1.41

Notes:

(i) b is a normalized propagation constant: $b = \frac{(\beta/k)^2 - n_2^2}{n_1^2 - n_2^2}$, where β = longitudinal propagation constant, $k = 2\pi/\lambda$.

(ii) Ai, Bi are Airy functions (58).

(iii) J denotes the Bessel function of the first kind (58).

with the achievement of built-in refractive index guides in the y-direction, Γ is a meaningful parameter and Equation 15.4 for the net gain G remains valid for cases of uniform gain g and loss α in the y-direction. For the symmetric graded-index real guides listed in Table 15.3 we will review the methods of calculating Γ and give results in the case of the lowest-order TE mode for the purpose of comparison with the results of the symmetric uniform-core (step-index) guide (case $c' = 0$ of Table 15.2 and Figure 15.2). Note that the definition of v remains as in (15.2) with stripe width $2S$ replacing layer thickness $2a$.

(a) *Linear*: In this case Γ may be evaluated directly in terms of the Airy functions and their derivatives, making use of a special property of these functions (57). The results are plotted in Figure 15.4; for values of v below about 2.5, Γ is slightly below the corresponding curve for the step-index profile (broken line).

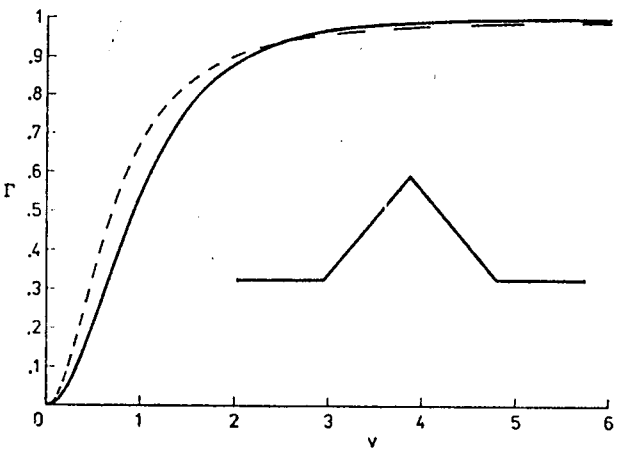

Figure 15.4 Γ versus v for the TE_0 mode of the symmetric linear profile (see inset); broken line gives the variation of Γ with v for the equivalent step-index guide

(b) *Extended-parabolic*: Computation of Γ for this profile is a straightforward integration over the Hermite-Gaussian field distributions. However, since this profile does not include the effects close to mode cut-off where the cladding layers would in practice provide a strong perturbation, no further results will be given here. Further results and a detailed critique of this profile as a laser waveguide model will be found in a recent publication (49).

(c) *Cladded-parabolic*: It is felt that this profile represents a more appropriate laser waveguide model than that of (b). Results using a series solution have been calculated here, although a number of possible other methods of analysis are available (see Reference 49 for a review). Plots of Γ versus v are given in Figure 15.5; for values of v below about 1.5, the graph lies just below that for the equivalent step-index guide (broken line).

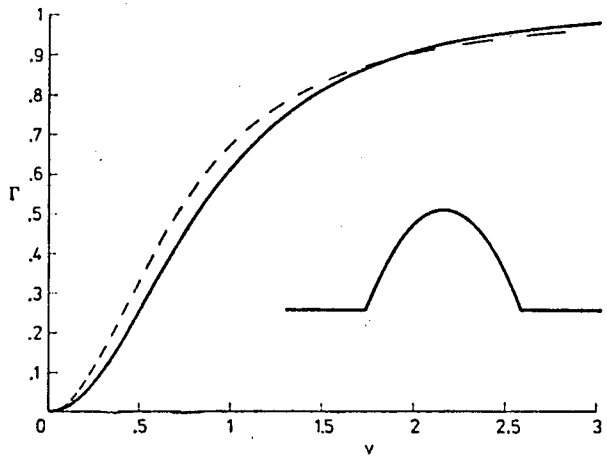

Figure 15.5 Γ versus v for the TE_0 mode of the symmetric cladded-parabolic profile (see inset); broken line gives the variation of Γ with v for the equivalent step-index guide

(d) *Exponential*: For this case Γ may be found as an integral over Bessel functions, which may be evaluated in terms of a series of Bessel functions (58). The results are given in Figure 15.6; once again the curve lies below the corresponding step-index result for a considerable range of v.

(e) *Sech-squared*: Although the field distributions take a reliability simple form for this profile, it is necessary to evaluate Γ by numerical integration. The results are shown in Figure 15.7 and again they lie just below those for the equivalent step-index curve for v less than about 3.

In view of the current interest in new laser structures for achieving good ranges of single-mode operation and 'kink'-free light-current curves, a further quantity of relevance is the value of v corresponding to cut-off of the first-order mode. The results for this quantity are given in Table 15.3 in the column

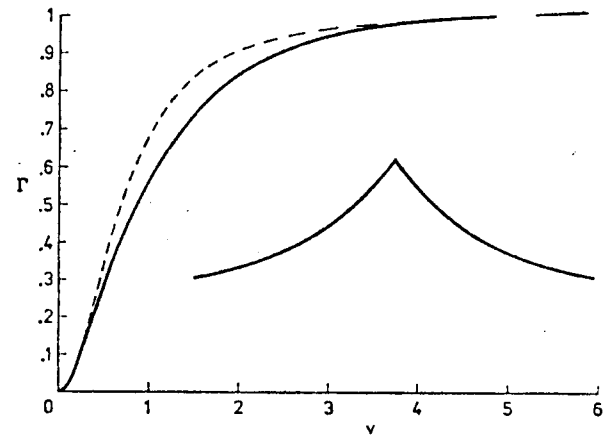

Figure 15.6 Γ versus v for the TE_0 mode of the symmetric exponential profile (see inset); broken line gives the variation of Γ with v for the equivalent step-index guide

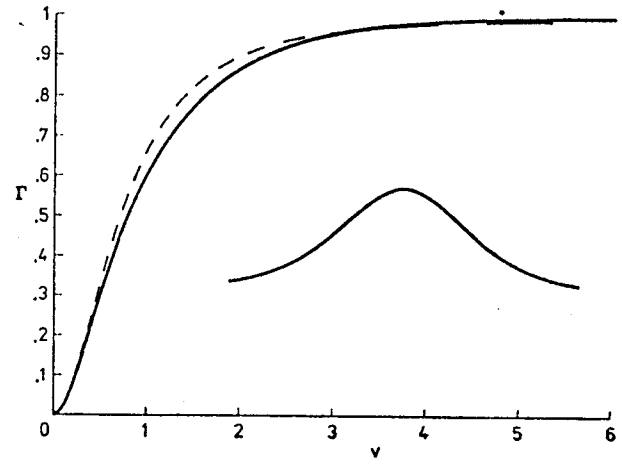

Figure 15.7 Γ versus v for the TE_0 mode of the sech-squared profile (see inset); broken line gives the variation of Γ with v for the equivalent step-index guide

headed 'v_{c1}'; from the Table the highest value of v_{c1} is seen to occur for the linear profile. A high value of v_{c1} is potentially advantageous in that a low value is difficult to achieve in practice, since very small values of either waveguide width or refractive index difference present technological problems. Note that although the results of Table 15.3 and Figures 15.4–15.7 were calculated for TE modes, there is approximate TE/TM degeneracy for sufficiently small values of the relative index difference Δ (28, 29). Finally, it should be emphasized that the results presented in this sub-section are for real dielectric waveguides and hence apply to injection lasers only in situations where the real waveguiding effect dominates over gain-guiding. Examples of such situations include the recent structures intended to yield linear output characteristics, such as the buried heterostructure (59), channelled substrate (60, 61), deep-diffused (62), and double stripe lasers (63). Discussion of the gain-guiding situation will be postponed until Section 15.3 below.

15.2.2.3 Spatial: z-direction

We will deal here with the description of the longitudinal photon field distributions in semiconductor lasers. Into this category falls also the subject of distributed-feedback (DFB) and distributed-Bragg-reflector (DBR) lasers, but these will not be discussed here: for an overview of these and related subjects the reader is referred to a recent review article (64).

At threshold and above the longitudinal photon field distribution $N(z)$ is composed of forward and backward travelling waves which may be summed to give a variation of the form (65, 66):

$$\frac{N(z)}{N(0)} = \cosh(zG) \tag{15.7}$$

where G is the (uniform) net gain per unit length (as in Equation 15.4 for the case of uniform gain transverse to the guide) and the origin of the z-axis is taken at the minimum of the field distribution. At threshold the value of G is conventionally given by the lasing threshold condition:

$$G = \frac{1}{2L}\ln\left(\frac{1}{R_1 R_2}\right) \tag{15.8}$$

where L is the cavity length and R_1, R_2 are the facet reflectivities. For a GaAs/air interface the reflectivities R_1 and R_2 are approximately 0.32, so that the maximum variation of longitudinal field distribution is given from (15.7) and (15.8) as $N(L/2)/N(0) = 1.17$. This variation is frequently neglected in calculations of laser properties; for lower values of R_1, R_2, as for example

in the case of anti-reflective coatings, the longitudinal variation of photon field distribution becomes more accentuated. Under these circumstances, since the electron and photon distributions are coupled, the electron distribution and hence the gain will no longer be uniform in the z-direction and more complicated interactions may occur (67, 68). A further discussion of these phenomena will be presented at the appropriate point in Section 15.3.

There is another source of non-uniform photon distribution in the z-direction: the standing wave structure of the field along the laser cavity (22). The length L of the cavity must be equal to an integer number of half-wavelengths. Since the longitudinal gain distribution is intimately coupled to the photon distribution, this results in a periodic variation of the gain along the cavity. This effect has recently become the basis of a theory concerning the reasons for multi-longitudinal-mode operation of injection lasers (69, 70). According to this theory, the non-uniform gain distribution permits other longitudinal modes to lase, provided that the carriers do not diffuse fast enough to smooth out the non-uniformity. Hence laser structures with lightly-doped active regions where both electrons and holes are injected (see Section 15.2.1.1 above) will tend to exhibit multimode oscillations since the ambipolar diffusion constant will be dominated by the slow diffusion of the hole concentration. On the other hand, structures with electron injection into heavily-doped active regions will tend to oscillate in fewer modes, since the electron diffusion constant is relatively large. Experimental observations on heavily-doped conventional double-heterostructures (70) and on TJS lasers (71) tend to support this explanation and yield single longitudinal mode operation over large ranges of drive current.

15.2.2.4 Temporal

To discuss the transient properties of injection lasers above threshold it is necessary to include the interaction of the photon field with the electron concentration n. In keeping with the spirit of our categorization of fundamental effects in Table 15.1, for the remainder of this sub-section the photon and electron distributions will be assumed spatially uniform. With this assumption, the rate equations describing multimode laser operation become (72–74):

$$\frac{\mathrm{d}n}{\mathrm{d}t} = \frac{j}{2ea} - \frac{R_{sp}}{\eta} - \sum_{i=1}^{M} \frac{c}{n_1} g_i N_i \tag{15.9}$$

$$\frac{\mathrm{d}N}{\mathrm{d}t} = \left(\frac{cg_i}{n_1} - \frac{1}{\tau_i}\right) N_i + \beta_i R_{sp} \tag{15.10}$$

where M is the number of modes, N_i, g_i, τ_i and β_i are respectively the photon density, gain, cavity lifetime and spontaneous emission factor of the ith mode, c is the speed of light, R_{sp} is the total spontaneous emission rate, η is the internal quantum efficiency, and the other symbols have been defined previously. Note the distinction between the electron concentration n and the refractive index n_1 in the equations. The effects of non-uniform spatial distributions of n and N, together with the appropriately modified versions of Equations 15.9 and 15.10 will be discussed in Section 15.3.

To proceed further with the solution of the rate Equations 15.9 and 15.10 it is necessary to find explicit expressions for the spontaneous emission rate R_{sp} and the gain g_i in terms of the electron concentration n. The calculation of such expressions falls within the topics to be covered in Section 15.2.2.5. However, the conventional approximation of an electron lifetime τ_n to describe the rate R_{sp}, and a phenomenological model for g_i, e.g. as a power-law dependence on n (75) permit the general form of the solutions to (15.9) and (15.10) to be explored. The existence of at least two time constants τ_n and τ_i gives rise to characteristic resonance frequencies associated with the solutions. For the case of single-mode oscillation ($M = 1$) a small-signal analysis yields for the resonance angular frequency ω_r (75):

$$\omega_r^2 = \frac{l}{\tau_n \tau_i}\left(\frac{j}{j_{th}} - 1\right) \tag{15.11}$$

where l is the index in the power-law expression for g_i and j_{th} is the threshold current density. The resonance frequency manifests itself in transient 'spiking' and quantum noise effects and also plays a key role in the understanding of high-frequency modulation of injection lasers. Under conditions of large-signal modulation the resonance shifts to lower frequencies (76–78) than given by the simple expression 15.11. At the same time the modulation efficiency decreases and a strong distortion of the modulated output may occur; these effects are confirmed experimentally (79).

The fraction of spontaneous emission into a lasing mode, denoted by β_i in Equation 15.10, has an important influence on the relaxation oscillations and 'ringing' effect in laser modulation (73, 74, 79–84). Large values of β_i (10^{-3}–10^{-2}), implying a large number of oscillating modes, would tend to damp the relaxation oscillations evoked in response to a step current pulse (80–83); they would also reduce the relative modulation amplitude at the resonance frequency ω_r (74, 81). In practice, experiments on stripe-geometry double-heterostructures have resulted in measured values of β_i in the range 10^{-5}–5×10^{-4} (74, 82), although there are also reports of β_i as high as 10^{-3}–10^{-2} (85, 86). A recent theoretical calculation of β_i (84) gave values around 10^{-5} for conventional GaAs laser parameters, and for the case of non-uniform photon distributions showed a linear dependence of β_i on the product of radiation confinement factors Γ_x, Γ_y (84, 79) defined for the x and y-directions as in Subsections 15.2.2.1 and 15.2.2.2. β_i is also found to be inversely-dependent on the volume of the active region, which may be a reason for the large β_i values, suppression of relaxation oscillations, and absence of resonance peaks in modulation characteristics of buried-heterostructure lasers (85).

The laser rate equations (15.9) and (15.10) have been used to study pattern effects in PCM of injection lasers. Pattern effects occur as a result (i) of the intrinsic time delay (23), (ii) of the values of electron population n and photon density N_i immediately before the application of a pulse (87), and (iii) the relaxation oscillations already discussed. Based on the theoretical analyses, suggestions for suppressing the pattern effects have been made; these include the use of compensation pulses (88), pre-biasing (89), pulse-shaping (90, 91), light injection (92–95), optical feedback (92), and resonant circuits (96). In all these cases the appropriate formulation of the rate equations including the spontaneous emission term in (15.10) is essential in order to permit accurate tracking of the electron and photon populations. In almost all cases, however, the assumption is made that all properties of the lasing modes are identical, so that the sum over modes in (15.9) can be replaced by the multiplicative constant M. A useful review of theoretical and experimental progress in the area of transient laser behaviour will be found in reference (79).

If Langevin noise operators are included in the rate equations 15.9 and 15.10 (97), then a detailed theory of the quantum noise in semiconductor lasers may be developed (98, 99). One important prediction of the theory is that the relative intensity noise should exhibit a maximum close to threshold and should decrease with increasing current above threshold. Experimental measurements by Paoli (100, 101) showed this stabilization in some lasers at low frequencies (< 100 MHz) but not at higher frequencies (> 2 GHz). This anomalous behaviour was tentatively attributed to long thermalization times so that the electron population could not respond quickly to the fluctuating photon density to provide quieting. However, the noise measurements of other authors (102–104) are in reasonable agreement with the theoretical predictions on this point. Further evidence of a lack of low-frequency noise stabilization above threshold has also been reported (105) and interpreted on the basis of spatially inhomogeneous gain saturation; the theoretical treatment of this problem will be discussed further in Section 15.3.

Recently, several authors (104, 106, 107) have published numerical solutions of the multimode rate equations including the Langevin noise terms, and have compared these results with the single-mode solutions. In general, the multimode case shows weaker intensity fluctuations than the single-mode situation for frequencies below resonance, the extent of the difference depending on the number of modes excited; near the resonance frequency the difference diminishes. For these calculations the properties of the modes are usually assumed identical; good qualitative agreement with experimental results has been achieved (104, 106, 107). A further development has been the extension of the theory to include the noise sources in the time-dependent equations when applied to direct modulation (108). The principal results is a shift of the noise peak to higher currents for increased modulation frequencies (shorter current pulse-widths), in general agreement with the experimentally-observed situation (108).

15.2.2.5 Spectral

In this subsection we will discuss the calculation of the spontaneous emission rate R_{sp} and the gain g as explicit functions of electron concentration n and, in the case of g, of photon energy E, for use in the rate equations 15.9 and 15.10. In the most general form, the expressions for these quantities are as follows (7, 72):

$$R_{sp} = \int_0^\infty r_{sp}(E)\mathrm{d}E \tag{15.12}$$

$$g(E) = \frac{\pi^2 c^2 \hbar^3}{n_1^2 E^2} r_{st}(E) \tag{15.13}$$

where

$$r_{st}(E) = r_{sp}(E)\left[1 - \exp\left(\frac{E - F_i + F_j}{KT}\right)\right] \tag{15.14}$$

$$r_{sp}(E) = \sum_{I,J} \frac{4n_1 e^2 E |M_{IJ}(E)|^2_{av}}{Vm^2\hbar^2 c^3} \varrho_{IJ}(E) f_I (1 - f_J)\, \delta_{E_I - E_J, E} \tag{15.15}$$

In these expressions, $\hbar$ is Planck's constant over 2π, K is Boltzmann's constant, T is the absolute temperature, m is the electron mass, F_i and F_j are quasi-Fermi levels associated with sets of energy states denoted by i and j, f_I and f_J are the Fermi–Dirac distribution functions associated with specific states I and J ($I \in i$, $J \in j$) of energies E_I and E_J, $\varrho_{IJ}(E)$ is the density of energy states contributing to emission of a photon of energy E, $|M_{IJ}(E)|^2_{av}$ is the square of the momentum matrix element for the I–J transition suitably arranged over

polarization and directions of the photon wave vector, V is the volume of the active region, and the rest of the symbols are as defined earlier.

The principal task in the evaluation of Equations 15.12–15.15 is to find suitable relations for the matrix element M_{IJ} and the density-of-states function ϱ_{IJ} for the transition of interest. The early history of calculations of this sort will be found in References 7 and 72. More recently, a rather comprehensive calculation has been presented by Casey and Stern (109) and applied to steady-state laser problems by Stern (110). This approach used the model of no k-selection rule for transitions between conduction and valence bands and their associated impurity band tails. The assumption of no k-selection rule is now fairly well-established and has found convincing experimental support (111). The density-of-states function ϱ_{IJ} thus becomes proportional to the product of density-of-states functions for each set of states i and j. The Casey–Stern model uses a density-of-states of the Kane form (25) to interpolate between the parabolic portions of the bands and the deep impurity tail states as described by the Halperin–Lax results (26). The optical matrix element M_{IJ} is calculated using empirically-determined wave functions which correctly reproduce the Bloch-like behaviour for states in the parabolic bands whilst reducing to the hydrogenic form for the localized states (24). For p-type GaAs these calculations give good agreement with experimental absorption data (109); the results are also in close accord with those from experimental studies of the spectral dependence of gain in heterostructure lasers (33, 112). A significant feature of Stern's results (110) is the confirmation that $R_{sp} = Bnp$ where B is reasonably independent of concentration at room-temperature and takes the value $\sim 2\times10^{-10}$ cm^{3}s^{-1} for GaAs.

Whilst the sophistication of this recent theoretical analysis (109, 110) provides excellent detail for the spectral and current dependence of the gain function in a uniform, steady-state laser model, it is also useful to have available approximate results for these quantities in order to use them in more complicated laser models allowing for non-uniformity, transience, etc. For these purposes it is, of course, possible to fit simple algebraic expressions to the numerical results for the quantities of interest. For example, the concentration dependence of gain g may be approximated by a simple power-law (75, 79, 95) as described in Section 15.2.2.4. Similarly, since the spectral dependence of g is only of interest in the region of its maximum, this may be modelled by a simple parabolic variation with energy E (20). Alternatively one may use approximations based on models of the transitions, densities-of-states, and matrix elements involved. One such approximation, based

loosely on the exponential band-tail model (72, 99) yields the formula

$$\frac{g(E,n)}{g_0} = \exp\left(\frac{E-E_G}{E_0}\right)\left[\ln\left(\frac{n}{n_0}\right)-\left(\frac{E-E_G}{E_0}\right)\right] \qquad (15.16)$$

where E_G is the band-gap, and E_0, n_0 and g_0 may be chosen to fit available results for $g(E, n)$, which may be theoretical (110) or experimental (111). It follows from Equation 15.16 that the gain maximum occurs at photon energy E_m, given by

$$\frac{E_m-E_G}{E_0} = \ln\left(\frac{n}{n_0}\right)-1 \qquad (15.17)$$

when the value of g is

$$\frac{g_m}{g_0} = \frac{n}{n_0}\exp(-1) \qquad (15.18)$$

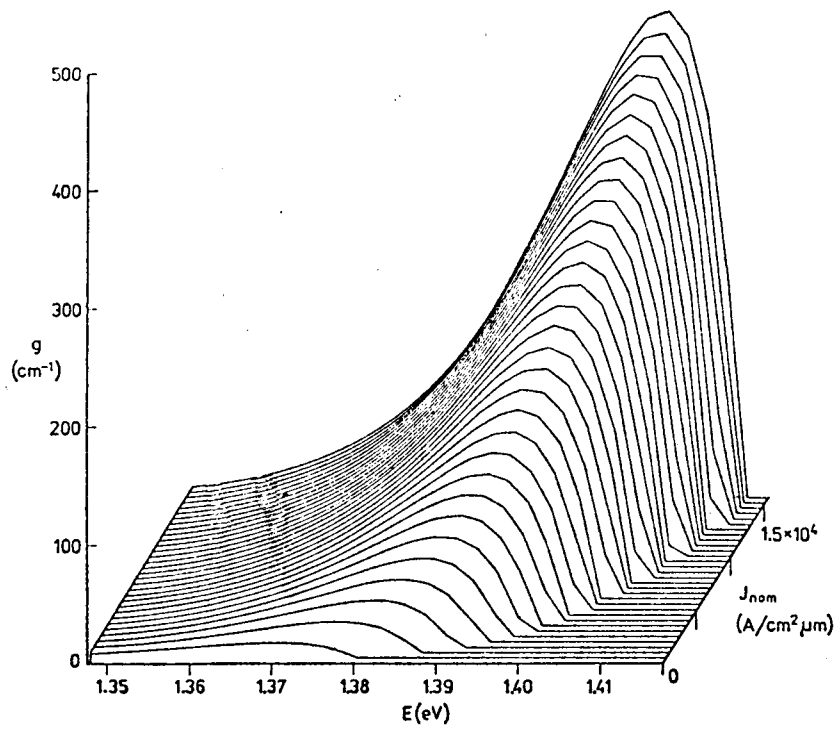

Figure 15.8 Gain g versus nominal current density J_{nom} (7, 110) and photon energy E from the simple model represented in Equation 15.16; parameters used were $E_0 = 10$ meV, $J_0 = 4\times10^4$ A/cm² μm, $g_0 = 2800$ cm^{-1}, $E_G = 1.424$ eV

If n is expressed in terms of Stern's nominal current density J_{nom} (7, 110) ($J_{nom} = 1.6\times10^{-23}Bnp = 1.6\times10^{-23}n/\tau_n$), then Equations 15.16–15.18 may be rewritten in terms of J_{nom} and an adjustable parameter J_0. Some results are given in Figure 15.8 in the form of a three-dimensional plot showing g as a function of E and J_{nom}. It should be emphasized that the simple model represented here cannot be expected to reproduce all the subtleties of more detailed numerical treatments (109, 110) but may be usefully applied in problems where the complications of non-uniformity and transient development are of interest. In this respect the model reasonably represents the main physical effects associated with the concentration and spectral dependencies of the gain.

15.2.3 Phonon effects

15.2.3.1 Spatial: x-direction

A primary source of heat in the semiconductor laser structure is non-radiative recombination occurring in the active region. Near threshold the power dissipated as heat at the junction is given approximately by ($jV_a 2SL$) where j is the current density, V_a is the applied voltage, $2S$ is the stripe width, and L is the laser length. In this expression the radiative output has been ignored and all electrical input power assumed converted to heat; other heat sources such as contact resistance, distributed bulk resistance, self-absorbed spontaneous emission, etc. have been neglected. If it is assumed that heat production is limited to a plane at the centre of the active layer and then flows in the x-direction to the heat-sink, then a simple one-dimensional solution of the heat-flow equation will describe the situation (113, 114). Such a model applied to oxide-insulated stripes (113), buried heterostructures (59) and mesa-structures, where heat flow in the y-direction may be neglected. The resulting temperature distribution through the layers from the active region to the heat-sink is amenable to comparison with experimental measurements (115, 116); in addition the model may be used to calculate the CW lasing range for given laser parameters (113, 114). The temperature gradient across many epitaxial layers with different thermal expansion coefficients may lead to a strain distribution (117) which may play a role in the initial degradation behaviour of lasers (118).

15.2.3.2 Spatial: y-direction

For structures other than those listed in the previous subsection, heat flow in the y-direction cannot be ignored. In these cases the Laplace equation for two-dimensional heat flow from a planar source situated in the active layer

is to be solved. The most general solutions take the form of Fourier transforms for a laser model assumed infinitely wide (119), and Fourier series for a model of finite width (120). The result is a temperature profile across the active area in the y-direction with a variation of typically a few degrees between the centre and edge of the stripe (120). Since the refractive index $n(y)$ of the active layer increases with temperature at the rate of $5 \times 10^{-4} K^{-1}$ (42), such a temperature profile may give rise to a corresponding refractive index profile with a positive guidance effect in the y-direction.

15.2.3.3 Spatial: z-direction

In the z-direction the conventional assumption is that the thermal distribution is uniform; the longitudinal expansion of a laser calculated on this basis agrees qualitatively with the result of measurements by an interferometric technique (115).

Another effect which falls into this category is a possible explanation of catastrophic degradation in high-power lasers. This is the excitation of acoustic waves by the optical radiation in the laser cavity (stimulated Brillouin emission) (121); according to this theory the acoustic phonons travel along the laser beam and cause damage ('burn-off') at the facets as a consequence of the weaker mechanical properties of the surfaces. However, it should also be noted that an alternative mechanism has been postulated to account for facet damage and catastrophic degradation, viz. optical absorption at inhomogeneities near the facet resulting in thermal runaway or a 'micro-explosion' (122).

15.2.3.4 Temporal

For pulsed operation with relatively short pulses ($\simeq$ 100 ns) the effects of heat diffusion away from the active region may be ignored and the heating may be assumed adiabatic. For this situation, the temperature rise ΔT of the active region in time t is given simply by (123):

$$\Delta T = \frac{jV_a SL}{\varrho C a} t \qquad (15.19)$$

where ϱ is the density, C the specific heat, and a the half-width of the active layer. For longer pulse widths it may be necessary to include thermal diffusion and find solutions to the time-dependent equation for heat conduction (123, 124). An associated phenomenon which has been reported is the existence of longitudinal and flexural vibrations attributed to shock heating and thermal expansion of the laser (117).

It is perhaps worth noting also in this sub-section that the combination of Equation 15.19 together with the thermal coefficient of refractive index noted in 15.2.3.2 leads to a mechanism for transient evolution of the refractive index of the active region. When this effect is considered in the context of a single-heterostructure laser where the guidance is very weak on the n-side, then it implies a time-dependent waveguide which may vary from below to above cut-off for the fundamental mode within the course of a current pulse. Such a mechanism has been invoked to account for long time delays and internal Q-switching in single heterostructure lasers (125); this latter model is to be contrasted with the other principal explanation of these phenomena, viz. that involving saturable absorption as the time-dependent 'driving force' leading to loss of optical confinement (126).

15.2.3.5 Spectral

Finally in this section we should include the fundamental features of phonon emission viewed as a non-radiative recombination route, i.e. as a mechanism causing reduced quantum efficiency η (as defined in Equation 15.9). The principal non-radiative mechanisms of this kind in laser materials are multi-phonon emission (127) and the Auger effect (128). Confining attention here to the former effect, a recent calculation (127) based on the configurational coordinate theory and applied to deep levels in GaAs yields values for the capture cross sections which may be as large as 10^{-14}–10^{-15} cm^2; experimental values also fall in this region (127).

15.3 SOME INTERACTIVE EFFECTS

In discussing the fundamental physical phenomena of Table 15.1, it has already been necessary to include some limited interaction between electrons, photons and phonons in order to give the description some validity. If we were to adopt a purely didactic approach it would now be possible to consider all interactive effects from the Table: 105 pairs, 455 triplets, etc.! However, within the limits of current or conceivable applications we are confined to rather fewer combinations. Since any limited choice must be largely determined by personal preference, I make no apology for restricting attention to the following four effects only.

15.3.1 Threshold calculations in symmetric double heterostructures

This simple example illustrates well the interactive nature characterizing the effects included in this section. The calculations of 15.2.2.1 provide the waveguide information, 15.2.2.4 the (steady-state) rate equations, and 15.2.2.5 the

gain-current relationship. For fundamental mode threshold, Equations 15.4, 15.8 and 15.18 provide the constitutive relations; if we include also the expression for the flow of carriers given in 15.2.1.1, then the threshold current density j_{th} is given by (in normalized variables):

$$j_{th} = Av\left[\left(\frac{1}{\Gamma}\right)\frac{1}{2L}\ln\left(\frac{1}{R_1R_2}\right)+\left(\frac{1}{\Gamma}-1\right)\alpha\right] \qquad (15.20)$$

where A is a constant and the other symbols are as defined previously.

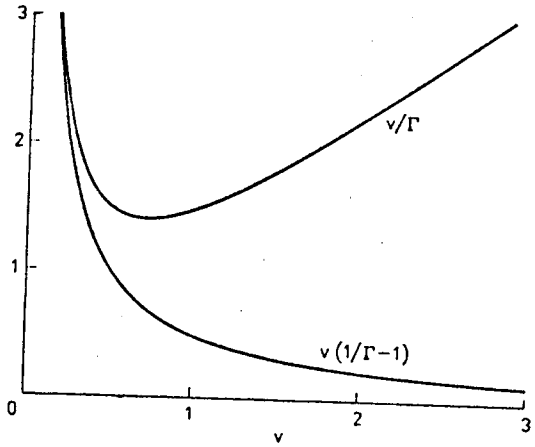

Figure 15.9 Threshold parameters v/Γ and $v(1/\Gamma-1)$ for the TE_0 mode of the three-layer slab waveguide plotted as functions of v

From the form of Equation 15.20 it is clear that all the waveguide information is contained in the normalized factors v/Γ and $v(1/\Gamma-1)$. Plots of these quantities versus v for the TE_0 mode of the symmetric three-layer slab waveguide ($c' = 0$ of Subsection 15.2.2.1) are given in Figure 15.9. Note that although Equation 15.20 was derived for the simple gain-current relationship of (15.18), it is a trivial extension to include the more general case $g_m \propto (n-n')$ (12, 112) where n' represents a carrier density necessary for cavity transparency. Hence Figure 15.9 may be said to contain all the necessary information for calculations of threshold current density when it is used in conjunction with an equation like 15.20. Whilst such calculations have already been presented in some detail for GaAs/GaAlAs lasers (30, 112, 129), the novelty of the present approach lies in the use of normalized variables, so that the results are easily

applied to new laser materials, e.g. those intended for use in optical communication systems at longer wavelengths where the absorption and dispersion properties of optical fibres are greatly improved (130). With reference to possible optimization of such materials it is also worth noting that for the simplest case where (15.20) applies and end-loss dominates strongly over α, the optimum v-value is given by the minimum of v/Γ on Figure 15.9 as $v = 0.71$ (131). For the conventional GaAs/GaAlAs double heterostructure with $n_1 = 3.6$ and $n_2 = 3.4$ this corresponds to an optimum active layer width of about 0.17 μm; when refractive index values of the newer laser materials become available, similar predictions of optimum layer thicknesses can be made. For example, for InGaAsP lasers grown on InP substrates (132), using measured InP refractive index data (133) and estimating the InGaAsP values from the effective band-gap shift (134), operation at $\lambda \simeq 1.3$ μm would imply an optimized active layer thickness of about 0.3 μm.

15.3.2 Guidance in stripe geometry lasers

Some discussion of this topic has already been given in Subsection 15.2.2.2 together with some considerations of real built-in guides; in addition, Subsection 15.2.3.2 included one mechanism for guidance under a conventional stripe contact, viz. a thermally-induced refractive index profile. However, there are also changes of real and imaginary parts of the dielectric permittivity associated with the injection of carriers underneath a stripe contact. Increased carrier density leads to an increase of gain (cf. Equation 15.18) and to a decrease of the refractive index (134, 135); in each case, to a first approximation, the variation is linear with electron density. Bearing in mind the remarks in 15.2.2.2 concerning dielectric profiles for which analytic solutions are available, it is therefore feasible to fit the electron distribution under the stripe to a profile whose modal solutions are well known. Figure 15.10 shows two such possible profiles—the extended-parabolic and sech-squared laws—which have been fitted to the electron distribution described by Equation 15.1. The parabolic profile was fitted to the small-signal expansion of (15.1) around $y = 0$ (19), whilst the sech-squared profile was matched to Equation 15.1 at $y = \pm S$; other methods of determining the appropriate fitting process have also been discussed in the literature (13, 38, 45). In view of Figure 15.10 and the remarks on the extended-parabolic profile in 15.2.2.2, it is clear that this distribution, although widely used in the literature (13, 19, 38, 41, 42, 136) is applicable only to modes well above cut-off which are largely confined to the central region under the stripe. The sech-squared profile, on the other hand, may be applicable for modes over a wide range, including close

to cut-off, and it is understood that an appropriate analysis is currently in progress (137).

Once a suitable model has been established for the dielectric distribution in the y-direction, this must be combined with the refractive index change

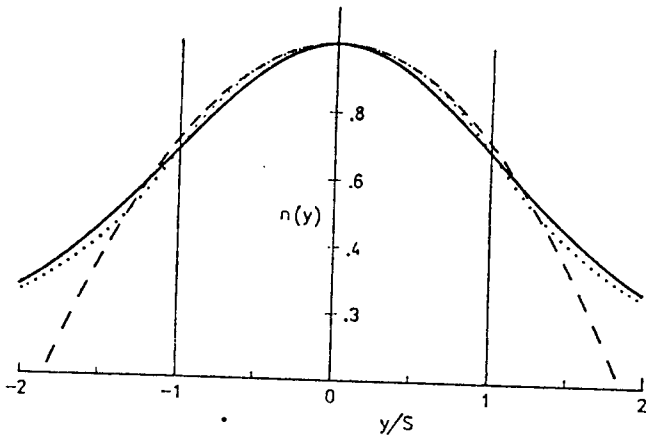

Figure 15.10 Carrier distributions under a stripe contact: *dotted line*—Equation 15.1 normalized to unity at $y = 0$, with $S/L_n = 1$; *solid line*—sech^2 profile, matched at $y = \pm S$; *dashed line*—parabolic approximation, fitted to small-signal expansion of (15.1) near $y = 0$

in the x-direction in order to find solutions to the wave equation in two dimensions. The most frequently used approximation for dealing with this problem is the effective dielectric permittivity method (138). The technique consists of replacing the actual two-dimensional dielectric distribution by an effective one-dimensional profile (19, 61, 135, 136, 138, 139), the solutions of which are usually fairly simple to obtain. For the stripe-geometry double heterostructure the guidance in the x-direction is usually much stronger than that in the y-direction where the dielectric profile is relatively slowly-varying. Hence the solution for the x-direction is usually obtained first (as discussed in Section 15.2.2.1) and then assumed to have a weak y-dependence; an effective dielectric permittivity may then be defined for the y-direction which incorporates the x-direction solutions. If the active and passive layer dielectric permittivities are denoted by $\xi_1(y)$ and $\xi_2(y)$, respectively, then the effective permittivity is given by (140)

$$\varepsilon_{eff}(y) = b\varepsilon_1(y) + (1-b)\varepsilon_2(y) \qquad (15.21)$$

where b is a (weakly y-dependent) normalized propagation constant (29) found from the x-direction field solutions as

$$b = \frac{(\beta/k)^2 - \varepsilon_2(y)}{\varepsilon_1(y) - \varepsilon_2(y)} \qquad (15.22)$$

and β is the longitudinal propagation constant. Solutions of the one-dimensional wave equation with permittivity given by (15.21) may then be used to calculate the net gain G of the laser. Allowing for the y-dependence of the gain of the active layer, $g(y)$, and the loss of the passive layers, $\alpha(y)$, the analogous equation to 15.4 becomes:

$$G = \Gamma \frac{\int_{-\infty}^{\infty} g(y)|\Phi(y)|^2 dy}{\int_{-\infty}^{\infty} |\Phi(y)|^2 dy} - (1-\Gamma)\frac{\int_{-\infty}^{\infty} \alpha(y)|\Phi(y)|^2 dy}{\int_{-\infty}^{\infty} |\Phi(y)|^2 dy} \qquad (15.23)$$

where Γ is the confinement factor for the x-direction guide and $\Phi(y)$ is the y-dependent part of the (separable) field solutions.

Calculations based on the model described in this subsection have been performed by Buus (140); rather than use approximations to the electron and dielectric distributions, his model was based on the calculated profiles and employed a numerical technique for solving the wave equation.

15.3.3 Longitudinal and transverse field distributions in stripe geometry lasers

A further degree of complexity is introduced into the problem of describing guidance associated with stripe contacts when the longitudinal variation of carrier and photon populations is included. Since the photon distribution is maximum at the facets (Equation 15.7) and the gain varies inversely with the photon population for a uniform current distribution (Equation 15.9), it follows that the gain distribution is minimum at the facets. If we consider, for simplicity, the case of gain-guiding only (40–42), then it becomes clear that the strength of guidance in the y-direction must vary along the cavity length, being at its weakest at the facets (141). To quantify these ideas, note that from Equations 15.7–15.9 in steady-state and for single-mode operation far above threshold (so that spontaneous emission may be ignored), a first approximation for the gain distribution $g(z)$ is given by (141)

$$g(z) = \frac{g(0)}{\cosh\left[\frac{z}{2L}\ln\left(\frac{1}{R_1 R_2}\right)\right]} \qquad (15.24)$$

For a z-dependent dielectric distribution such as that given in (15.24), solutions to the scalar wave equation may be found by the method of Kogelnik

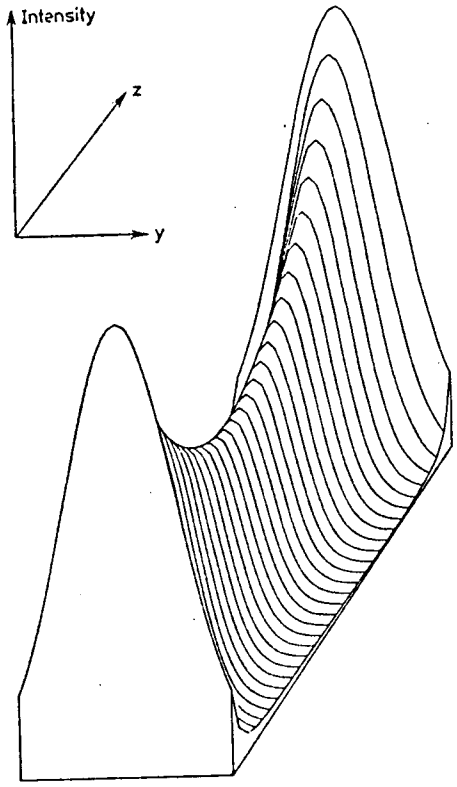

Figure 15.11 Photon field intensity distribution in the y- and z-directions calculated for a 10 μm stripe-geometry GaAs laser with facet reflectivities of 0.05 and cavity length 500 μm

(142). Assuming a parabolic variation for g in the y-direction and using the effective index approach to allow for guidance in the x-direction, it is then possible to calculate the photon field distribution as a function of all three spatial coordinates. The results differ significantly from those assuming uniformity in the z-direction, especially for low values of facet reflectivity R_1, R_2. A typical result is shown in Figure 15.11, where the photon field intensity is plotted as a function of y and z for $R_1 = R_2 = 0.05$ and $L = 500$ μm. As anticipated from the arguments given above, the field is best confined in the lateral direction near the centre of the cavity and spreads to its maximum breadth at the mirrors; the corresponding distribution of the gain is shown in Figure 15.12.

For stripe-geometry lasers, especially with anti-reflection coated facets, it follows from this theory (141) that:

(a) For the gain-guiding situation the fields are spread at the laser facets, hence giving a lower power density which may assist in inhibiting both catastrophic (121, 122) and long-term degradation (143).

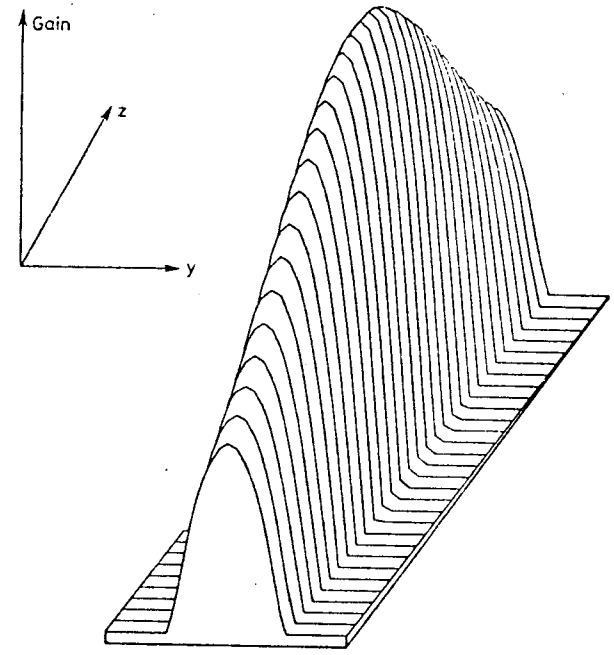

Figure 15.12 Distribution of gain corresponding to the field variation of Figure 15.11

(b) In the opposite situation of real guidance produced either by dips in the carrier concentration (spatial hole burning (15, 19)) or by a specific fabrication process, the behaviour will be reversed in that the fields will be strongly focused at the facets; similar calculations to those presented above support this. An analogous situation may exist in the x-direction in high-power single-heterostructure lasers.

(c) Experiments designed to study guidance mechanisms in a.r.-coated lasers (42) should be interpreted with caution, lest the effect of the non-uniform z-variation masks the mechanism operating in the y-direction.

(d) The interactive effect studied here could in principle be used to produce specific distributions of the laser output beam by suitable profiling of the stripe contact along the length of the laser (141).

15.3.4 Transient evolution of spatial and spectral distributions of photons and electrons

In this subsection we shall include the temporal and spectral variation of the photon and electron concentrations; in other words, non-uniformity is allowed in all five rows of Table 15.1. An adequate description is given by allowing all terms in the rate equations 15.9 and 15.10 to be functions of x, y, z, t, and, where appropriate, photon energy E. A certain amount of simplification is achieved by recalling from 15.2.1.1 that the carrier concentrations are usually constant across the active layer, so that the equations may be averaged over x. A further logical step is to average the photon rate equation also over y (144) and z (22), so that the photon density N becomes a function only of t. The rate equations then assume the form (20, 79, 86):

$$\frac{dn(y,z,t)}{dt} = \frac{j}{2ea} + D_n\left(\frac{\partial^2}{\partial y^2}+\frac{\partial^2}{\partial z^2}\right)n(y,z,t) - \frac{R_{sp}(n)}{\eta} - \frac{c}{n_1}\sum_{i=1}^{M}\Gamma_i g_i(E_i,n)N_i(t)|\Phi(y,z)|^2 \qquad (15.25)$$

$$\frac{dN_i(t)}{dt} = \frac{c}{n_1}N_i(t)\left\{\Gamma_i\frac{\int g_i(E_i,n)|\Phi(y,z)|^2dydz}{\int|\Phi(y,z)|^2dydz} - (1-\Gamma_i)\frac{\int\alpha(E_i,y,z,t)|\Phi(y,z)|^2dydz}{\int|\Phi(y,z)|^2dydz}\right\} - \frac{N_i(t)}{\tau_i} + \Gamma_i\frac{\pi^2c^3\hbar^3}{Vn_1^2E^2}\frac{\int r_{sp}(E_i,n)|\Phi(y,z)|^2dydz}{\int|\Phi(y,z)|^2dydz} \qquad (15.26)$$

where all the symbols are as defined previously. In particular, Γ_i is the confinement factor in the x-direction for mode i, E_i is the photon energy of mode i, $\Phi(y,z)$ is the normalized field amplitude, and $g_i(E_i,n)$, $r_{sp}(E_i,n)$, and $R_{sp}(n)$ are the corresponding gain, spontaneous emission rate, and total spontaneous rate (integrated over photon energy). Note that a comparison of Equations 15.10 and 15.26 may be used to obtain an expression for the spontaneous emission factor β_i (84). The second term in Equation 15.25 allows for lateral and longitudinal diffusion of electrons (20, 22, 79, 86, 145). Equation 15.26 has been derived on the assumption that the cavity lifetime

τ_i is independent of position; it usually corresponds to the end-loss which is given explicitly in Equation 15.8. In the steady-state and ignoring spontaneous emission, Equation 15.26 may be used to calculate lasing thresholds, when it becomes equivalent to the combination of Equations 15.8 and 15.23 with the z-dependence neglected. Note also that the mode index i in (15.25) and (15.26) may apply to transverse, lateral, and longitudinal mode numbers.

For single-mode operation the rate equations 15.25 and 15.26 have been solved numerically by Cross (146). In this analysis the effects of diffusion were ignored in (15.25), the loss term α in (26) was assumed constant, and the effects of spontaneous emission on the lasing mode (last term in (15.26)) were neglected; in addition longitudinal uniformity was assumed (no z-dependence). The results indicated the usual 'spiking' oscillations in response to a step current pulse, with the additional feature of a corresponding oscillation in field distribution in the y-direction; a time-dependent real waveguide in the y-direction was assumed as a consequence of the fluctuating carrier density (see Section 15.3.2). These results have recently been confirmed by experimental studies of broad oxide-stripe lasers (17–20 μm) (147).

When multimode operation is permitted in the rate equations 15.25 and 15.26, the response to a step current pulse is more complicated. Since the electron concentration overshoots its equilibrium value during the relaxation oscillations, the gain is temporarily sufficient for a number of modes to be above threshold. When the number of modes is increased, the power in the dominant mode is consequently reduced. The net effect is a spectral broadening which decreases with increasing time after the onset of the current pulse; detailed theoretical analyses have been made by Ikegami (148) and Buus *et al.* (20, 86). This broadening (of order 3 nm) may also occur in sinusoidal modulation and PCM (79, 148, 149) where it might be a severe limitation on the bandwidth of an optical communications system, as a result of material dispersion in the fibre. The effect is diminished somewhat by diffusion of carriers, which tends to favour the dominant mode (20, 22, 86, 145, 148), or by a high rate of spontaneous emission into the modes (see Section 15.2.2.4). It may be controlled by external light injection (73, 92–95) or by biasing the laser above threshold (150).

Equations similar to 15.25 and 15.26 but ignoring the z-dependence, have also been used to study the low-frequency intensity noise in CW stripe-geometry lasers (105). For two oscillating modes with different thresholds, the results indicate a lack of quieting above threshold owing to spatially-inhomogeneous gain saturation; this result is in qualitative agreement with experimental finding (see Section 15.2.2.4).

15.4 CONCLUSION

This contribution has been concerned with theoretical descriptions of the phenomena occurring in semiconductor lasers. We have seen in Section 15.2 that almost all the fundamental physical effects are now amenable to theoretical analysis and, in Section 15.3, that the prime areas of current concern are associated with interactive effects involving one or more of the possible combinations from Table 15.1. In the areas of wave-guidance, the design of new laser structures, and transient phenomena, the theoretical descriptions have contributed strongly to the mainstream of semiconductor laser development. A possible exception to this rule has been the subject of long-term degradation studies, where an understanding of some of the fundamental mechanisms is still outstanding, in spite of the enormous effort which has been invested.

It is perhaps appropriate to conclude by listing a few specific effects of current interest where further theoretical study could be profitable:

(i) *Guidance in stripe-geometry lasers.* There are at least five mechanisms influencing the guidance in the y-direction:

(a) thermally-induced variation of the refractive index (120, 151),
(b) gain-guiding due to injected carriers (40–42),
(c) index-antiguiding associated with carrier distribution (19, 38),
(d) spatial hole-burning (self-focusing) in broad stripe lasers (6, 19, 38, 135, 146),
(e) strain effects associated with the contact (38).

A comprehensive understanding of the relative roles played by these mechanisms has not yet been achieved; in particular, the reported existence of guiding action even below lasing threshold (136, 151) poses a new challenge to theoretical analysis. An associated problem would be the description of the facet reflectivities and far-field patterns associated with these mechanisms; the presence of gain-guidance and astigmatic beams implies that these quantities are functions of injected current density.

(ii) *New laser structures.* Structures with a built-in waveguide in the y-direction are now being designed (59–63, 71, 152–154) with the objectives of stable single-mode operation and 'kink'-free output characteristics. In many cases these designs utilize the effective permittivity concept (described in 15.3.2) to analyse the strength of guidance obtained in a given structure. A point that arises is therefore concerned with the accuracy of this technique; other than a comparison with numerical solutions for the step-index guide

(138), there has been no effort to estimate the accuracy of the effective permittivity method or its applicability to a given situation.

(iii) *New laser materials for long-wavelength operation.* In this respect there is now a similar situation to that for the AlGaAs system some years ago; the waveguide theories available seem adequate, but there is as yet little refractive index data available. Hence there is a place for theoretical models of refractive indices in new laser materials, perhaps based on those available for AlGaAs (134, 155).

(iv) *Degradation problems.* To select only two particular areas where theoretical study seems appropriate, consider (a) self-pulsing observed in degraded lasers (156), and (b) effects of facet coating in improving laser lives (143). Whilst the former effect has been tentatively attributed to microscale absorption centres (157), an extremely large absorption cross section is necessary to explain the observed pulsations via repetitive Q-switching (158). As regards (b), the problem is to explain why facet coating is effective when half-wave films are used (159, 160) which do not intentionally change the facet reflectivity or limit the optical field intensity. An improved understanding of these phenomena may shed further light on the mechanisms responsible for laser degradation.

It is anticipated that theoretical work on the topics listed here and on related subjects will continue to play an important part in semiconductor laser development.

ACKNOWLEDGEMENTS

I am indebted to J. Buus for a preprint of Reference 140, and to the U.K. Science Research Council for the award of a research fellowship.

REFERENCES

1. See, for example, W. R. Frensley and H. Kroemer, *Phys. Rev.*, B, **16**, 2642 (1977), and references therein.
2. C. M. Garner, Y. D. Shen, J. S. Kim, G. L. Pearson, W. E. Spicer, J. S. Harris, Jr., and D. D. Edwall, *J. Appl. Phys.*, **48**, 3147 (1977).
3. B. N. Sharapov, *Soviet Physics-Semiconductors*, **4**, 948 (1970); also *Fiz. Tekh. Poluprov.*, **4**, 1121 (1970).
4. R. D. Burnham, P. D. Dapkus, N. Holonyak, Jr., D. L. Keune, and H. R. Zwicker, *Solid State Electronics*, **13**, 199 (1970).

5. K. A. Shore, *Quarterly Report No. 2 on Post Office Contract No. 541509* (1972).
6. B. W. Hakki, *J. Appl. Phys.*, **45**, 288 (1974).
7. F. Stern, in *Laser Handbook*, ed. F. T. Arecchi and E. O. Schulz-DuBois (North-Holland, Amsterdam, 1974) pp. 425–440.
8. K. A. Shore and M. J. Adams, *Optical and Quantum Electronics*, **8**, 269 (1976).
9. D. L. Rode, *J. Appl. Phys.*, **45**, 3887, (1974).
10. A. R. Goodwin, J. R. Peters, M. Pion, G. H. B. Thompson, and J. E. A. Whiteaway, *J. Appl. Phys.*, **46**, 3126 (1975).
11. K. A. Shore and M. J. Adams, *App. Phys.*, **9**, 161 (1976).
12. B. W. Hakki, *J. Appl. Phys.*, **44**, 5021 (1973).
13. B. W. Hakki, *J. Appl. Phys.*, **46**, 2723 (1975).
14. W. P. Dumke, *Solid State Electron.*, **16**, 1279 (1963).
15. B. W. Hakki, *J. Appl. Phys.*, **46**, 292 (1975).
16. I. Ladany, *J. Appl. Phys.*, **48**, 1935 (1977).
17. N. Chinone, *J. Appl. Phys.*, **48**, 3237 (1977).
18. A. S. Logginov and V. E. Solovev, *Phys. stat. sol.* (a), **41**, 371 (1977).
19. P. A. Kirkby, A. R. Goodwin, G. H. B. Thompson, and P. R. Selway, *IEEE Jnl.*, QE-13, 705 (1977).
20. J. Buus and M. Danielsen, *IEEE Jnl.*, QE-13, 669 (1977).
21. H. S. Sommers, Jr., and D. O. North, *J. Appl. Phys.*, **48**, 4460 (1977).
22. H. Statz, C. L. Tang, and J. M. Lavine, *J. Appl. Phys.*, **35**, 2581 (1964).
23. K. Konnerth and C. Lanza, *Appl. Phys. Letts.*, **4**, 120 (1964).
24. D. M. Eagles, *J. Phys. Chem. Solids*, **16**, 76 (1960).
25. E. O. Kane, *Phys. Rev.*, **131**, 79 (1963).
26. B. I. Halperin and M. Lax, *Phys. Rev.*, **148**, 722 (1966).
27. For a review, see E. Göbel and M. H. Pilkuhn, *J. de Physique*, **35**, C3-191 (1974).
28. W. W. Anderson, *IEEE* Jnl., QE-1, 228 (1965).
29. H. Kogelnik and V. Ramaswamy, *Appl. Opt.*, **13**, 1857 (1974).
30. I. Hayashi, M. B. Panish, and F. K. Reinhart, *J. Appl. Phys.*, **42**, 1929 (1971).
31. M. J. Adams, *Optics Commun.*, **23**, 105 (1977).
32. G. H. B. Thompson and P. A. Kirkby, *IEEE Jnl.*, QE-9, 311 (1973).
33. G. H. B. Thompson, G. D. Henshall, G. E. A. Whiteaway, and P. A. Kirkby, *J. Appl. Phys.*, **47**, 1501 (1976).
34. H. C. Casey, Jr., M. B. Panish, W. O. Schlosser, and T. L. Paoli, *J. Appl. Phys.*, **45**, 322 (1974).
35. H. C. Casey, Jr., S. Somekh, and M. Ilegems, *Appl. Phys. Letts.*, **27**, 142 (1975).
36. A. Aiki, M. Nakamura, J. Umeda, A. Yariv, A. Katzir, and H. W. Yen, *Appl. Phys. Letts.*, **27**, 403 (1975).
37. D. R. Scifres, W. Streifer, and R. D. Burnham, *Appl. Phys. Letts.*, **29**, 23 (1976).
38. G. H. B. Thompson, D. F. Lovelace, and S. E. H. Turley, *Solid-State and Electron Devices*, **2**, 12 (1978).
39. M. Cross and M. J. Adams, *Solid-State Electron.*, **15**, 919 (1972).
40. W. O. Schlosser, *B.S.T.J.*, **52**, 887 (1973).
41. F. R. Nash, *J. Appl. Phys.*, **44**, 4696 (1973).
42. D. D. Cook and F. R. Nash, *J. Appl. Phys.*, **46**, 1660 (1975).
43. P. S. Epstein, *Proc. Nat. Acad. Sci.*, **16**, 627 (1930).

44. S. N. Stolyarov, *Sov. Jnl. of Quantum Electron.*, **2**, 144 (1972); also *Kvant. Elektr.*, 2, 69 (1972).
45. M. Osinski, *Opt. and Quantum Electron.*, **9**, 361 (1977).
46. D. Marcuse, *IEEE Jnl.*, QE-9, 1000 (1973).
47. W. W. Rigrod, J. H. McFee, M. A. Pollack, and R. A. Logan, *J.O.S.A.*, **65**, 46 (1975).
48. W. Streifer, R. D. Burnham, and D. R. Scifres, *IEEE Jnl.*, QE-12, 494 (1976).
49. M. J. Adams, *Opt. and Quantum Electron.*, **10**, 17 (1978).
50. E. M. Conwell, *Appl. Phys. Letts.*, **23**, 328 (1973).
51. J. R. Carruthers, I. P. Kaminov, and L. W. Stulz, *Appl. Optics*, **13**, 2333 (1974).
52. H. A. Haus and R. V. Schmidt, *Appl. Optics*, **15**, 774 (1976).
53. H. Kogelnik, in *Integrated Optics*, ed. T. Tamir (Springer-Verlag, N.Y., 1975) pp. 13–81,
54. D. F. Nelson and J. McKenna, *Jnl. of Appl. Phys.*, 38, 4057 (1967).
55. O. V. Bogdankevich, V. S. Letokhov, and A. F. Suchkov, *Sov. Phys.-Semiconductors*, 3, 566 (1969); also *Fiz. Tekh. Poluprov.*, **3**, 665 (1969).
56. K. Unger, *Ann. Physik*, **19**, 64 (1967).
57. J. A. Arnaud and W. Mammel, *IEEE Trans.*, MTT-23, 927 (1975).
58. M. Abramowitz and I. A. Stegun, *Handbook of Mathematical Functions*, Dover, N.Y., 1965.
59. T. Tsukada, *J. Appl. Phys.*, **45**, 4899 (1974).
60. R. D. Burnham and D. R. Scifres, *Appl. Phys. Lett.*, **27**, 510 (1975).
61. P. A. Kirkby and G. H. B. Thompson, *J. Appl. Phys.*, **47**, 4578 (1976).
62. H. Yonezu, Y. Matsumoto, T. Shinohara, I. Sakuma, T. Suzuki, K. Kobayashi, R. Lang, Y. Nannichi, and I. Hayashi, *Japan. Jnl. Appl. Phys.*, **16**, 209 (1977).
63. P. A. Kirkby, A. R. Goodwin, and R. S. Baulcomb, presented at the conference 'Semiconductor Injection Lasers and their Applications', Cardiff, Wales, 1977.
64. A. Yariv and M. Nakamura, *IEEE Jnl.*, QE-13, 233 (1977).
65. Y. Nannichi, *J. Appl. Phys.*, 37, 3009 (1966).
66. R. Ulbrich and M. H. Pilkuhn, *IEEE Jnl.*, QE-6, 314 (1970).
67. C. H. Gooch, in *Proceedings of the International Symposium on* GaAs (Institute of Physics, London, 1966), pp. 62–67.
68. S. Hasuo and T. Ohmi, *Japan. Jnl. Appl. Phys.*, **13**, 1429 (1974).
69. W. Streifer, R. D. Burnham, and D. R. Scifres, *IEEE Jnl.*, QE-13, 403 (1977).
70. D. R. Scifres, R. D. Burnham, and W. Streifer, *Appl. Phys. Letts.*, **31**, 112 (1977).
71. H. Namizaki, *IEEE Jnl.*, QE-11, 427 (1975).
72. M. J. Adams and P. T. Landsberg, in *Gallium Arsenide Lasers*, ed. C. H. Gooch (Wiley, London, 1969), pp. 5–79.
73. H. Hillbrand and P. Russer, *Electron. Letts.*, **11**, 372 (1975).
74. Y. Suematsu, S. Akiba, and T. Hong, *IEEE Jnl.*, QE-13, 596 (1977).
75. M. J. Adams, *Opto-electronics*, 5, 201 (1973).
76. T. Ikegami and Y. Suematsu, *Electronics and Communications in Japan*, 53-B6,
77. W. Harth, *Electron. Letts.*, 9, 532 (1973).
78. W. Harth, *A.E.U.*, 29, 149 (1975).
79. G. Arnold and P. Russer, *Appl. Phys.*, **14**, 255 (1977).
80. P. M. Boers, M. T. Vlaardingerbroek, and M. Danielsen, *Electron. Letts.*, **11**, 206 (1975).
81. W. Harth and D. Siemsen, *A.E.U.*, 30, 343 (1976).
82. J. Angerstein and D. Siemsen, *A.E.U.*, 30, 477 (1976).
83. K. Kajiyama, S. Hata, and S. Sakata, *Appl. Phys.*, **12**, 209 (1977).

84. Y. Suematsu and K. Furuya, *Trans. IECE*, E60, 467 (1977).
85. T. Kobayashi and S. Takahashi, *Japan. Jnl. Appl. Phys.* **15**, 2025 (1976).
86. J. Buus, M. Danielsen, P. Jeppesen, F. Mengel, M. Moeskjaer, and V. Ostoich, *Proceedings of the Second European Conference on Optical Fibre Communication* (1976), pp. 231–239.
87. T. Ozeki and T. Ito, *IEEE Jnl.*, QE-9, 388 (1973).
88. T. Ozeki and T. Ito, *IEEE Jnl.*, QE-9, 1098 (1973).
89. T. P. Lee and R. M. DeRosier, *Proc. IEEE*, 62, 1176 (1974).
90. J. G. Farrington and J. E. Carroll, *Proceedings of the First European Conference on Optical Fibre Communications* (1975), pp. 135–137.
91. M. Danielsen, *IEEE Jnl.*, QE-12, 657 (1976).
92. K. Kobayashi, R. Lang, and K. Minemura, *Japan. Jnl. Appl. Phys.*, **15**, 281 (1976).
93. P. Russer, *A.E.U.*, 29, 231 (1975).
94. R. Lang and K. Kobayashi, *IEEE Jnl.*, QE-12, 194 (1976).
95. P. Russer, G. Arnold, and K. Petermann, *Proceedings of the Third European Conference on Optical Fibre Communication* (1977), pp. 139–141.
96. Y. Suematsu and T. Hong, *IEEE Jnl.*, QE-13, 756 (1977).
97. D. E. McCumber, *Phys. Rev.*, **141**, 306 (1966).
98. H. Haug, *Phys. Rev.*, **184**, 338 (1969).
99. D. J. Morgan and M. J. Adams, *Phys. stat. sol.* (a), **11**, 243 (1972).
100. T. L. Paoli, *Appl. Phys. Letts.*, **24**, 187 (1974).
101. T. L. Paoli, *IEEE Jnl.*, QE-11, 276 (1975).
102. G. Guekos, H. Jäckel and K. F. Schmid, *Electron. Letts.*, **12**, 64 (1976).
103. H. Jäckel, *Electron. Letts.*, **12**, 289 (1976).
104. H. Jäckel and G. Guekos, *Opt. and Quantum Electron.*, **9**, 233 (1977).
105. R. Lang, K. Minemura, and K. Kobayashi, *Electron. Letts.*, **13**, 228 (1977).
106. M. Danielsen, J. Buus, F. Mengel, K. Mortensen, and K. Stubkjaer, *Proceedings of the Third European Conference on Optical Communications*, (1977), pp. 142–144,
107. T. Ito, S. Machida, K. Namata, and T. Ikegami, *IEEE Jnl.*, QE-13, 574 (1977).
108. W. R. Lange, *Electron. Letts.*, **14**, 7 (1978).
109. H. C. Casey, Jr., and F. Stern, J. Appl. Phys., **47**, 631 (1976).
110. F. Stern, J. Appl. Phys., **47**, 5382 (1976).
111. See, for example, E. O. Goebel, O. Hildebrand, and K. Löhnert, *IEEE Jnl.*, QE-13 848 (1977).
112. B. W. Hakki and T. L. Paoli, *J. Appl. Phys.*, **46**, 1299 (1975).
113. J. C. Dyment, J. E. Ripper, and T. H. Zachos, *J. Appl. Phys.*, **40**, 1802 (1969).
114. P. Garel-Jones and J. C. Dyment, *IEEE Jnl.*, QE-11, 408 (1975).
115. R. Keller, R. Salathé, and T. Tschudi, *IEEE Jnl.*, QE-8, 783 (1972).
116. T. Kobayashi and Y. Furukawa, *Japan. Jnl. Appl. Phys.*, **14**, 1981 (1975).
117. R. Keller, C. Voumard, and H. Weber, *Appl. Phys. Letts.*, **26**, 50 (1975).
118. C. J. Hwang, *Appl. Phys. Letts.*, **30**, 167 (1977).
119. H. Yonezu, I. Sakuma, K. Kobayashi, T. Kamejima, M. Ueno, and Y. Nannichi, *Japan. Jnl. Appl. Phys.*, **12**, 1585 (1973).
120. W. B. Joyce and R. W. Dixon, *J. Appl. Phys.*, **46**, 855 (1975).
121. H. Kressel and H. Mierop, *J. Appl. Phys.*, **38**, 5419 (1967).
122. C. D. Dobson and F. S. Keeble, *Proceedings of the International Symposium on Gallium Arsenide* (London, The Institute of Physics and the Physical Society, 1967), pp. 68–71.

123. R. S. Broom, *IEEE Jnl.*, QE-4, 135 (1968).
124. W. Nakwaski, *Electron. Technology* (Poland), **9**, 2 (1976).
125. F. D. Nunes, N. B. Patel, and J. E. Ripper, *IEEE Jnl.*, QE-13, 675 (1977).
126. See, for example, M. J. Adams and B. Thomas, *IEEE Jnl.*, QE-13, 580 (1977), and references therein.
127. C. H. Henry and D. V. Lang, *Phys. Rev.*, B15, 989 (1977).
128. For a review, especially with reference to GaAs, see P. T. Landsberg and M. J. Adams, *J. Luminescence*, **7**, 3 (1973).
129. H. Kressel and M. Ettenberg, *J. Appl. Phys.*, **47**, 3533 (1976).
130. For a recent review, see T. Kimura and K. Daikoku, *Opt. and Quantum Electron.* **9**, 33 (1977).
131. H. G. Unger, *A.E.U.*, **25**, 539 (1971).
132. J. J. Hsieh, J. A. Rossi, and J. P. Donnelly, *Appl. Phys. Letts.*, **28**, 709 (1976).
133. G. D. Pettit and W. J. Turner, *J. Appl. Phys.*, **36**, 2081 (1965).
134. M. J. Adams and M. Cross, *Solid State Electronics*, **14**, 865 (1971).
135. G. H. B. Thompson, *Optoelectronics*, **4**, 257 (1972).
136. T. L. Paoli, *IEEE Jnl.*, QE-13, 662 (1977).
137. M. Osinski, private communication.
138. For a recent account, together with references to the relevant literature, see G. B. Hekker and W. K. Burns, *Applied Optics*, **16**, 113 (1977).
139. T. Rozzi, T. Itoh, and L. Grun, *Radio Science*, **12**, 543 (1977).
140. J. Buus, ~~to be published~~. IEEE Jl. QE-15, 734 (1979).
141. M. J. Adams, *Electron. Letts.*, **13**, 236 (1977).
142. H. Kogelnik, *Appl. Optics*, **4**, 1562 (1965).
143. H. Kressel and I. Ladany, *R.C.A. Rev.*, **36**, 230 (1975).
144. J. E. Carroll, S. G. Eldon, and G. H. B. Thompson, *Electron. Letts.*, **12**, 564 (1976).
145. K. Otsuka, *IEEE Jnl.*, QE-13, 520 (1977).
146. M. Cross, *Phys. stat. sol.* (a), **16**, 167 (1973).
147. P. R. Selway, P. A. Kirkby, A. R. Goodwin, and G. H. B. Thompson, *S.S.E.D.*, **2**, 38 (1978).
148. T. Ikegami, *Proceedings of the First European Conference on Optical Fibre Communication* (1975), pp. 111–113.
149. G. Arnold, F.-J. Berlec, and R. Petschacher, *Proceeding of the Third European Conference on Optical Fibre Communication* (1977), pp. 136–138.
150. P. R. Selway and A. R. Goodwin, *Electron. Letts.*, **12**, 25 (1976).
151. J. E. Ripper, F. D. Nunes, and N. B. Patel, *Appl. Phys. Letts.*, **27**, 328 (1975).
152. K. Aiki, M. Nakamura, T. Kurada, and J. Umeda, *Appl. Phy. Letts.*, **30**, 649 (1977).
153. L. Figueroa and S. Wang, *Appl. Phys. Letts.*, **31**, 45 (1977).
154. L. Figueroa and S. Wang, *Appl. Phys. Letts.*, **32**, 55 (1978).
155. M. A. Afromowitz, *Solid State Commun.*, **15**, 59 (1974).
156. T. L. Paoli, *IEEE Jnl.*, QE-13, 351 (1977).
157. D. Kato, *Appl. Phys. Letts.*, **31**, 588 (1977).
158. M. J. Adams, *Phys. stat. sol.* (a), **1**, 143 (1970).
159. I. Ladany, M. Ettenberg, H. F. Lockwood, and H. Kressel, *Appl. Phys. Letts.*, **30**, 87 (1977).
160. Y. Shima, N. Chinone, and R. Ito, *Appl. Phys. Letts.*, **31**, 625 (1977).